Intracavity CO laser photoacoustic trace gas detection: cyclic CH_4, H_2O and CO_2 emission by cockroaches and scarab beetles

F. G. C. Bijnen, F. J. M. Harren, J. H. P. Hackstein, and J. Reuss

A liquid-nitrogen-cooled CO laser and an intracavity resonant photoacoustic cell are employed to monitor trace gases. The setup was designed to monitor trace gas emissions of biological samples on line. The arrangement offers the possibility to measure gases at the 10^9 by volume (ppbv) level (e.g., CH_4, H_2O) and to detect rapid changes in trace gas emission. A detection limit of 1 ppbv for CH_4 in N_2 equivalent to a minimal detectable absorption of 3×10^{-9} cm^{-1} can be achieved. Because of the kinetic cooling effect we lowered the detection limit for CH_4 in air is decreased to 10 ppbv. We used the instrument in a first application to measure the CH_4 and H_2O emission of individual cockroaches and scarab beetles. These emissions could be correlated with CO_2 emissions that were recorded simultaneously with an infrared gas analyzer. Characteristic breathing patterns of the insects could be observed; unexpectedly methane was also found to be released.

Key words: CO laser, photoacoustics, trace gas, methane, water, insects.

1. Introduction

Infrared photoacoustic (PA) spectroscopy is one of the most sensitive techniques that one can use to measure low trace gas concentrations under atmospheric conditions.[1] CO_2 lasers have been employed for excitation predominantly because of their high output power in the infrared (900–1100 cm^{-1}) and their relative ease of operation. Optimizing the PA signal can be achieved by the cell design and intracavity laser operation. Other laser sources employed to detect photoacoustically atmospheric trace gases are He–Ne[2,3] and diode lasers.[4] In comparison the CO_2 laser possesses broad tunability and high laser power permitting measurements of mixtures of several gases at (sub)-part per billion volume concentrations (1 part per billion = $1{:}10^9$).[5]

The conditions for high laser power and broad line tunability are also met by a CO laser. In particular the liquid-nitrogen-cooled ($\Delta V = 1$) CO laser is line tunable over a large frequency range (350 lines between 1200 and 2100 cm^{-1}),[6–8] in which many gases possess a strong fingerprint absorption for their fundamental vibration modes. Furthermore, it is also possible to use the CO laser on $\Delta V = 2$ (300 laser lines), thereby reaching the range from 2450 to 3800 cm^{-1}.[9]

Previously,[10] a cw CO laser was employed in a PA arrangement to monitor car exhaust gases. Multiline emission and water vapor absorption generated problems and made it necessary for one to use a dual-beam arrangement with a reference system. To avoid multiline emission the laser must be cooled from the 265 K used by Bernegger and Sigrist[10] to a liquid-nitrogen temperature of 77 K.[11] This yields higher population densities, resulting in laser action for the lower J levels from $P(6)$ to $P(13)$ compared with the 265 K CO laser that functions mainly between $P(13)$ and $P(24)$. The rovibrational population is distributed over fewer and lower rotational levels, which causes less overlap between adjacent vibrational transitions resulting in single-line lasing conditions for almost all laser lines. Since the population density is higher for the lower-lying rotational levels, the population difference between the lasing levels is also larger. Therefore, laser action occurs even at weak vibrational transitions, yielding

F. G. C. Bijnen, F. J. M. Harren, and J. Reuss are with the Department of Molecular and Laser Physics, University of Nijmegen, Toernooiveld, 6525 ED Nijmegen, The Netherlands. J. H. P. Hackstein is with the Department of Microbiology and Evolutionary Biology, University of Nijmegen, Toernooiveld, 6525 ED Nijmegen, The Netherlands.

Received 10 October 1995; revised manuscript received 3 April 1996.

0003-6935/96/275357-12$10.00/0

an extended wavelength range from 1260 cm^{-1} ($V = 35 \rightarrow 34$) to 2080 cm^{-1} ($V = 3 \rightarrow 2$).[6–8]

We focus on the performance and characteristics of the liquid-nitrogen-cooled CO laser and an intracavity PA cell. We optimized the PA cell to detect fast changes of low production sources of CH_4 and H_2O. The experimental setup is applied to monitor trace gas release from single insects.

Atmospheric CH_4 contributes significantly to the process of global warming and ozone depletion. Biogenic sources are responsible for the major part of the mondial CH_4 flux (>70%); the contribution of each different source is still a question for debate.[12] Some arthropods (i.e., millipedes, cockroaches, termites, and scarab beetles) are believed to contribute as much as 25% of the total production.[13] Gas chromatography allows measurement of the methane release of single animals only after incubation for several hours. Consequently these measurements cannot provide information about the dynamic character of the gas emission. Infrared absorption measurements yield fast response times and permit observation of the dynamics of CO_2 emissions.

In addition to CH_4 and CO_2 emissions of insects, water vapor release has been the subject of many studies. Information about water loss dynamics in insects is based on theoretical modeling, sensitive weighing, and relatively slow direct water vapor measurements.[14–17]

Cockroaches at rest show a regular breathing pattern that is postulated to reduce water loss and optimize O_2 uptake.[14] This breathing is accomplished by a complicated sequence of opening and closing of the spiracle valves of the tracheal system and by venting the content of the tracheae through abdominal motions. We monitored the H_2O and CH_4 release, together with the CO_2 emission, during the complete sequence of fluttering, ventilation, and constriction for the cockroach species *Periplaneta americana* and *Gromphadorhina portentosa* and for the scarab beetle *Pachnoda bhutana.*

2. CO Laser

Inside the plasma discharge of the CO laser, inelastic electron scattering produces states of excitation of low-lying vibrational N_2 and CO molecules. By collisional transfer of vibrational energy from N_2 to CO the population of the lower vibrational states of carbon monoxide is further enhanced. Because of the vibrational anharmonicity of the electronic ground state, $X^1\Sigma$, the spacing of the vibrational levels decreases as V increases. By energy pooling collisions CO molecules are therefore pushed further up the vibrational ladder. Because of this V–V or Treanor pumping one can reach high-lying vibrational levels.[18] The pumping is more effective when the translational temperature of the discharge is low. The rotational temperature is closely coupled to the translational temperature but the vibrational population is entirely athermal and possesses the so-called Treanor plateau ($V = 7$ to $V = 36$). We can assign an effective temperature only to parts of the vibrational distribution. For the Treanor plateau a typical temperature of 20,000 K can be ascribed.[19] Consequently partial population inversion can occur; the higher vibrational state ($V + 1$) with the lower rotational quantum number ($J - 1$) is more populated than the (V, J) state. Corresponding P-type transitions are observed to show laser action.

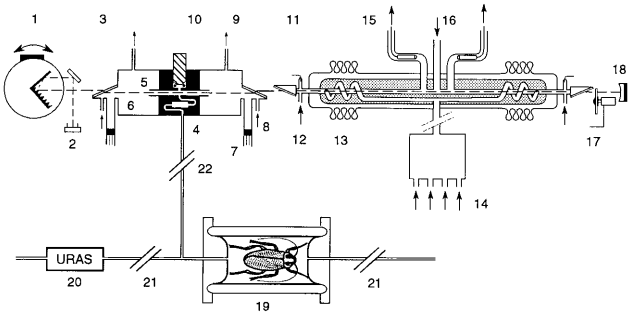

Fig. 1. CO laser detection setup in combination with a PA cell: 1, grating to select the appropriate transition; 2, power meter at zero-order reflection of the grating; 3, PA cell; 4, inlet for trace gas running through a quarter lambda notch filter; 5, resonator tube; 6, buffer volume; 7, tunable side arm to minimize window signal; 8, inlet for buffer gas; 9, outlet for buffer gas and trace gas; 10, microphone; 11, CO laser; 12, helium flow to flush the windows; 13, liquid-nitrogen jacket; 14, He, CO, N_2, and air mixing barrel in front of laser gas inlet; 15, laser gas outlet toward pump; 16, N_2 flow to start laser discharge at start of measurement; 17, chopper; 18, 100% reflecting mirror (R = 10 m); 19, cuvette containing insect; 20, infrared gas analyzer (URAS); 21, 22, cooling traps to remove water vapor for CH_4 measurements.

The experimental arrangement is shown in Fig. 1. With some minor changes the liquid-nitrogen-cooled CO laser tube is based on the design of Wu *et al.*[8] and has been constructed in our workshop. When the gas mixture was optimized for an optimal laser power on a weak laser line [$P(10)_{32}$, 1304.97 cm^{-1}] laser operation was achieved between 1260 and 2000 cm^{-1} on 250 lines in one single scan (see Fig. 2). Intracavity laser power amounts to 40 W (1920 cm^{-1}). In the long wavelength region of the emission spectrum

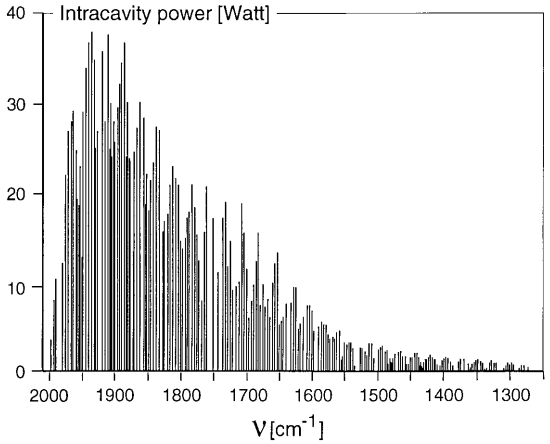

Fig. 2. 250 CO laser lines between 1260 and 2000 cm^{-1} (7.7 and 5.0 μm). Note that lines around 1750 cm^{-1} are missing because of water vapor absorption.

many lasing transitions could be operated at an intracavity power of 1 W. The operating pressure of our discharge was typically 10 mbar. For long wavelength operation the laser gas mixture consisted of 8 mbar of He, 1.5 mbar of N_2, 0.6 mbar of CO, and less than 0.1 mbar of air. Since the optimum gas mixtures for laser action above 2000 cm^{-1} differ drastically from those in the long wavelength region, at least two different gas mixtures are necessary to cover the full range from 1260 ($V = 35 \rightarrow 34$) to 2080 cm^{-1} ($V = 3 \rightarrow 2$). Short wavelength operation could be obtained mainly by decreasing the CO concentration; the absence of collisional energy pooling achieves population at low-lying vibrational levels.

Optimal laser action at a single laser line was achieved by adjustment of the electrical current and consequently the (rotational) temperature of the plasma; a low current yielded high powers at low J values. Helium served as a cooling agent in the laser gas mixture. Levels of nitrogen or helium were less critical than that of oxygen. Because of its low ionization potential the latter lowers the electron temperature in the discharge thereby improving the vibrational excitation of CO and N_2.[20] Too much O_2 caused fast vibrational–translational relaxation, resulting in a lower gain. Oxygen also impeded dissociation of CO; dissociation into carbon can be observed as blackening of the discharge tube wall. In our case, a thin brown film was observed after several days of continuous operation. Although we did not experience detrimental effects of this layer on the laser operation, we removed it as part of our standard cleaning procedure by means of a helium–air discharge at room-temperature burning for several hours.

The Pyrex discharge tube (11.4-mm diameter, 1.3-m length) with an active discharge length of 1.16 m was surrounded by a liquid-nitrogen bath thermally shielded by a vacuum jacket. The laser gas mixture was precooled by liquid nitrogen before it entered the discharge tube. The precooling path was approximately 0.7 m long, however a simple experiment showed that a length of 40 mm would have been sufficient to cool the gas to liquid-nitrogen temperature at the flow rates applied. Invar rods provided a rigid mount for the grating and the 100% reflecting mirror ($R = 10$ m); the overall length of the cavity was 2.2 m.

The discharge tube had two ZnSe Brewster windows. The windows were continuously flushed by a small helium flow to avoid contamination by the discharge. Nitrogen could also be used as a flushing gas; however because of its lower ionization potential helium has little influence on the operating conditions of the laser.

A vacuum pump was used to force the laser gas mixture through the laser discharge tube, longitudinally from the sides to the center. For our CO laser an 8-m^3/h pump was employed. A pump with half of this pumping capacity resulted in less lines and approximately 40% less power on the strongest laser lines. We tested two other pumps with a higher capacity but this resulted in only a slight increase (typically 10%) of laser power. In view of gas consumption the 8-m^3/h pump was chosen.

The laser power was monitored on the zero-order reflection of the grating. We used a concave mirror to focus this radiation on a pyroelectric detector. The grating (230 lines/mm blazed at 5.5 μm) was operated in first-order reflection and showed strong output losses in zero order at both extreme wavelength regions of the laser transitions (at 1260 and 2080 cm^{-1}), thereby limiting laser operation.

The dc laser discharge was driven by a current-stabilized high-voltage power supply (FUG, Rosenheim, Germany). The negative high-voltage output was split into two branches (Fig. 1), each containing resistors of approximately 2.3 MΩ to balance the negative impedance of the laser discharge; these branches were connected to the center cathodes. A high ballast resistance allowed the laser to be operated at low currents. It was advantageous to perform long-term measurements since liquid nitrogen consumption was reduced.

The center cathodes were separated from each other by a distance of 100 mm to prevent excitation of only one of the two branches. If the gas balance was not optimal (e.g., due to a small gas leak in one of the branches) the discharge conditions were less favorable and the discharge could not be started in both branches. To overcome this problem an additional inlet for N_2 was placed in the center of the laser tube. Since the ionization potential of nitrogen is higher than that of the laser gas mixture the discharge was forced to split to both branches. When the discharge worked on both sides, the nitrogen flow at the center stopped; the discharge remained in both arms.

Both anodes were grounded and were positioned at the ends of the laser tube. This configuration was more advantageous than the one described previously.[8,11] Only one high-voltage power supply was necessary and, in addition, the intracavity PA cell and the chopper could be positioned close to the windows of the laser since the outer anodes were at ground potential.

The axial liquid-nitrogen jacket around the laser tube was automatically refilled to allow for long-term measurements. For a typical electric current density of 4 mA/cm^2 the consumption of liquid nitrogen was approximately 4 L/h. We were able to operate the CO laser continuously for five days. During this period the intracavity power at, e.g., 1304.97 cm^{-1} decreased by a factor of 2. This was due to the deposition of solid CO_2 as a film on the cooled inner wall of the laser discharge tube.

3. Photoacoustic Cell

The PA effect is based on conversion of electromagnetic to acoustic energy. In our case, modulated infrared CO laser radiation was absorbed by trace gases (e.g., CH_4) in air or N_2. By way of collisional relaxation the vibrational energy of periodically excited molecules was transferred to translational energy, which gave rise to pressure modulation.

Inside the PA cell a longitudinal resonator optimally sustained this ensuing periodic pressure modulation and a condenser microphone mounted at the antinode of the resonator was used to monitor the sound. The resonator was acoustically separated from the windows by buffers. Depending on the length and radius of the resonator this type of configuration leads, in general, to a high cell constant (10^3–10^4 Pa cm/W). The cell constant is a measure for the sensitivity expressed as the acoustic pressure amplitude resulting from a normalized quantity of energy absorbed over the length of 1 cm by the trace gas. Notwithstanding the high sensitivity a relatively low Q factor results ranging between 10 and 100. To avoid temperature drifts of the cell that are due to replenishment of the laser with liquid nitrogen, by use of a control unit we maintained the cell temperature at 23 °C, which is just above the temperature of the laboratory.

The PA cell was placed inside the CO laser cavity to profit from the order of magnitude power increase compared with an extracavity position. The cell was positioned close to the grating near the minimum waist of the laser beam; the 100% reflecting silver-coated mirror (R = 10 m) was used to focus the beam on the grating. The frequency stability demands were easily met by our chopper (0.2%). For intracavity laser operation an asymmetric blade (60% open) was employed. The chopping frequency corresponded to an acoustic wavelength of twice the length of the resonator. The chopper positioned at the mirror side of the laser cavity produced sound and mechanical vibrations coherent with the modulated infrared radiation. These coupled through the Invar rods and the body of the PA cell and yielded a constant background signal. We reduced the coupling by maximizing the distance of the chopper blade to any object in its vicinity. With the blade mounted to the driving motor axis one could turn it freely in space without acoustic shielding. We obtained a further reduction of coupling by mounting the chopper and PA cell onto vibrational dampers that were attached to the Invar rod frame. At the acoustic resonance of the PA cell, this resulted in a constant background signal of 3 μPa, which is just above the detection limit of the detector.

The dimensions of the resonator and the resulting acoustic characteristics of the cell are listed in Table 1. For the acoustic resonator we chose a small radius, which is preferable since it results in a higher cell constant.[21] A radius of 6 mm proved to be too small; an unstable background signal was observed that was due to wall heating by the wings of the Gaussian beam. We reached a good compromise by increasing the resonator radius to 7.5 mm. Choosing a long resonator length results in a higher cell constant and would be advantageous. On the other hand, a short resonator length reduced the overall size of the arrangement. Additionally a small volume of the resonator could yield a fast sequence of consecutive independent measurements (time response). As a compromise we chose the length of 150 mm resulting in a resonance frequency of 1010 Hz for air at STP conditions and a time response of 15 s at a typical flow of 5 L/h.

Table 1. Characteristic Dimensions and Performance of the PA Cell

Resonator diameter and length	15 × 150 mm
Buffer diameter and length	100 × 100 mm
Resonance frequency (in N_2 at STP)	1030 Hz
Quality factor (Q)	40 ± 2
Sensitivity B&K 4179 microphone	1 V/Pa
Intrinsic noise level microphone	200 nPa Hz^{-1}
Acoustic background noise	2 μPa Hz^{-1}
Cell constant (F)	(2.0 ± 0.1) × 10^3 Pa cm/W
Sensitivity photoacoustic cell (1-W laser power)	(3.0 ± 0.2) × 10^{-9} cm^{-1}

Since absorption of (scattered) laser radiation can periodically heat up the resonator wall, we tested four resonators, each of a different material or with a different surface treatment, for their suitability to yield a low background signal. Material and surface quality for the resonators are listed in Table 2. To investigate experimentally the influence of the material properties we directed a 1-W cw CO_2 waveguide laser beam at 943.34 cm^{-1} to the center of the resonators at a grazing incidence angle of 3.2 deg. Expressed in terms of equivalent gas absorption amplitude the PA signal arising from wall absorption can be found in Table 2. The unpolished gold-coated copper tube produced a threefold higher signal than the polished version.

The relatively low absorption amplitude of the polished gold-coated copper resonator, compared with those made from stainless steel and brass, can be understood by comparing the bulk properties of the metals. PA signal generation is proportional to $(\kappa c_p)^{-1/2}$ with κ as the thermal conductivity and c_p as the heat capacity of the bulk material. For stainless steel, brass, and copper this resulted in a ratio of, respectively, 6:2:1. This ratio was approximately observed. The best performance was obtained by employing a copper tube as resonator material with a polished gold coating. Because of the excellent heat-conducting properties the absorbed heat can be quickly dispersed in the copper tube. The gold coating served not only to optimize

Table 2. Experimental PA Background Signals Compared with Bulk Properties of Various Materials and Surface Qualities[a]

Material	Experimental	Bulk Properties $(\kappa c_p)^{-1/2}$
Polished stainless steel	3	6
Polished brass	2.5	2
Polished gold-coated copper	1	1
Unpolished gold-coated copper	3.5	1

[a]We obtained the results by monitoring the PA signal generated by an amplitude-modulated CO_2 waveguide laser beam directed at the center of the resonator at grazing incidence. Values are scaled to the results of the polished gold-coated resonator.

the reflection of laser radiation, but also to obtain a noncorrosive surface to withstand aggressive gases.

Another source of acoustic background signal resulted from radiation absorbed by the ZnSe window material. Two measures were employed to minimize this background signal (Fig. 1). The first was the use of large buffer volumes between the resonator and the window. Since the trace gas flow was introduced directly to the center of the resonator this hardly affected the time response of the detector. The second was the introduction of tunable air columns close to the windows as described previously.[22,23]

The performance of the cell was tested with an extracavity CO_2 waveguide laser beam modulated by a chopper. The laser beam passed through the first, transparent, ZnSe Brewster window and was partially absorbed in the slightly blackened second window. By tuning the air column at this window we observed a clear maximum at 60-mm and a minimum at 80-mm column lengths in the PA window signal. The window signal could even be reduced by a factor of 40 compared with the situation when there was no air column. A theoretical model has been developed to describe this acoustic behavior.[22,23] The results of this model predicted a reduction factor of 50 for the window signal amplitude at a column length of 80 mm. Placing the PA cell into the laser cavity with optimally transparent windows, we observed hardly any effect on the low background signal amplitude by changing the column length. Apparently, the large buffers sufficed to minimize the window signal.

The acoustic signal originating from absorption was monitored by a Bruel & Kjaer (B&K) 4179 condenser microphone. The membrane of the microphone and the volume in front of it were part of the acoustic resonance, thereby influencing the resonance frequency, cell constant, and quality factor.[22,23] The use of a small electret Knowless EK 3024 microphone did not show a measurable influence. The above-mentioned theoretical model was applied to clarify this effect. The results corresponded well with the experimental data and could explain the downshift in resonance frequency by 65 Hz. The B&K microphone was advantageous because we used its high signal-to-noise ratio to lower the detection limit.

The lowest nonelectronic noise level can be determined by the Brownian motion of the molecules and poses a limit to the sensitivity of this detector. Although the cell was shielded and mounted to the laser frame on vibrational dampers we did not reach the theoretical limit (0.2 μPa $Hz^{-1/2}$) because acoustic noise (2 μPa $Hz^{-1/2}$) was picked up at the resonance frequency, which limited the sensitivity of the system. We therefore could not yet utilize the full potential of the B&K microphone. In the case of trace gas detection of methane in N_2 this pickup noise restricted the practical detection limit to 1 ppbv (absorption coefficient $\alpha = 3$ atm^{-1} cm^{-1} at 1304.97 cm^{-1}, 1-W laser power, see Fig. 3).

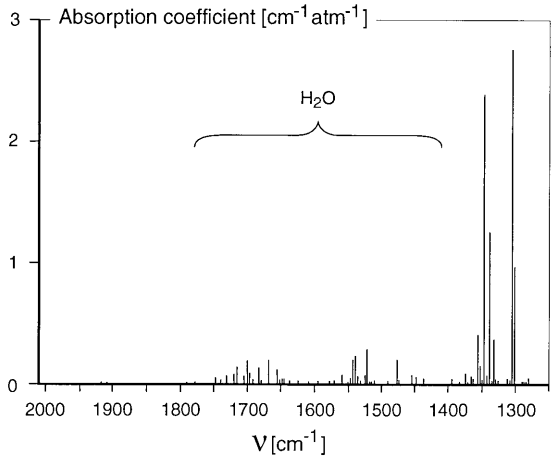

Fig. 3. Absorption spectrum of CH_4 in N_2 for CO laser transitions. Because of the strong water vapor absorption between 1400 and 1750 cm^{-1} and strong wall adsorption of water vapor, some water absorption can still be observed.

4. Detection of Methane in N_2 and Air

By injecting 1 mL of N_2 containing 1 nL of CH_4 into a carrier flow of dry air we observed that, at the 1304.97-cm^{-1} laser line, the acoustic signal was 1 order of magnitude lower than for pure N_2 as the carrier flow. Furthermore, in air a phase lag of 150 deg occurred compared with the case when a small amount of ethylene (1445.46-cm^{-1} laser wavelength) or ethane (1493.81 cm^{-1}) was injected and measured. The phase lag indicated that energy was taken up and stored temporarily by the molecules in the resonator at the modulation frequency of 1030 Hz instead of yielding directly modulated kinetic energy release. This effect is known as kinetic cooling and is well documented for CO_2 absorption in the CO_2 laser wavelength region.[24,25]

In our case, CH_4 absorbed the CO laser radiation in the ν_4 vibrational mode centered around 1306.2 cm^{-1}. This is the lowest vibrational mode of the molecule; the collisional relaxation lifetime is therefore large compared with other molecules with a smaller energy gap between their lowest vibrational modes and their ground state. The adjacent ν_2 mode (1533.3 cm^{-1}) will also become thermally populated (rate constant 13 μs^{-1} atm^{-1}).[26] Oxygen has a near-resonant vibrational ν_1 level (1554 cm^{-1}). Only 170 collisions are needed to transfer energy from the ν_3 mode of CH_4 to the ν_1 mode of O_2 (rate constant $\approx$28 μs^{-1} atm^{-1}).[27] Since this is a somewhat fast process probably most of the energy is deposited into O_2 and then relaxes slowly; the average number of collisions (Z_{10}) required for relaxation of an O_2 molecule from the ν_1 state to the ground state is 8.3×10^7 in pure O_2. At STP conditions some 5×10^9 collisions/s take place. The much larger number density of O_2 compared with CH_4 creates a buffer of vibrational energy leading to an effective transient cooling of the translational degrees of freedom. Because of our fast modulation frequency (1010 Hz) we observed this transient cooling by O_2 as an amplitude decrease and

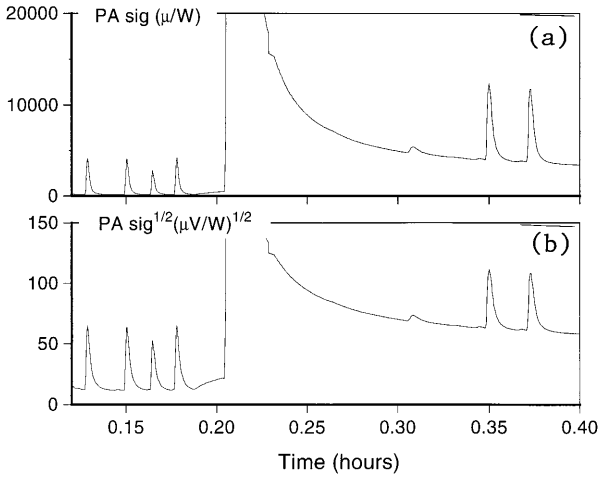

Fig. 4. (a) PA signal at the $P(11)_{19}$ CO laser line resulting from injections of equal amounts (1-mL air containing 2.6% water vapor) either on top of a low or on top of a high water vapor concentration. The injections on the high background result in a larger PA signal. The large background is caused by a cockroach in the cuvette. (b) Square root of the PA signal; the integrated surface under all the peaks is equal.

a phase change relative to the signal caused by the same level of CH_4 in N_2.

In the case of pure carrier gas N_2 ($\nu_1 = 2330\ cm^{-1}$), kinetic cooling can hardly take place because of the large energy gap with respect to the excited vibrational mode of CH_4.

Water vapor is known to promote vibrational relaxation and, indeed, by increasing the humidity of the flow we increased the PA signal amplitude from methane absorption substantially and reduced the phase lag. It is therefore preferable to measure the methane release from insects at high humidity conditions. However, to allow the water vapor release from insects to be measured the experiments are normally performed in dry air conditions. Our results did not allow us to determine whether water vapor promoted relaxation of CH_4 or O_2.

Ethylene and ethane were also tested, but we observed no change of their trace gas signal by introducing extra water vapor into the flow. The introduction of water vapor into the flow yields only a slightly higher background signal arising from water absorption ($\alpha \approx 10^{-5}\ atm^{-1}\ cm^{-1}$) at the $P(10)_{32}$ CO laser line that was used for CH_4 detection.

5. Water Vapor Detection in the Presence of Oxygen

Water vapor has a strong absorption band (ν_2 at 1594.7 cm^{-1}) in the CO laser region. To prevent overload of the detector we did not use one of the strongest water vapor absorption lines, e.g., $P(12)_{13}$ (1761.69 cm^{-1}, $\alpha \approx 2\ atm^{-1}\ cm^{-1}$), but a moderate absorbing line $P(11)_{19}$ (1616.04 cm^{-1}, $\alpha \approx 0.3\ atm^{-1}\ cm^{-1}$). In the case of air as a carrier gas a quadratic dependence on the H_2O concentration was found. Figure 4(a) shows the PA signal as a result of several injections of 1-mL N_2, containing 2.6% of water vapor, into the carrier flow. When the injections (ΔP) were performed on a large PA water vapor background signal (P) the total PA signal (S) was much larger compared with injections on a low water vapor background signal. Taking the square root resulted in equally sized peaks as shown in Fig. 4(b). Although water vapor is known to be a fast relaxing agent, O_2 apparently acted again as buffer for vibrational energy storage that could then be released by collisions with water vapor molecules yielding a nonlinear concentration dependence. Fast relaxation of O_2 is to be expected at high water vapor concentrations; in this case the PA signal is linear with the concentration. Further experiments have to be performed in order to elucidate this problem.

Because of the strong adsorption of water molecules to wall material and because of its spectral interference with other gases, outgassing of water vapor from walls could perturb the performance of the detector. We reduced the outgassing problem by inserting a cooling trap and perfluoroalkoxy (PFA) Teflon tubing into the gas-handling system between the sampling cell and the PA cell. In this way we were able to lower the water background signal below 1 ppmv. A detection limit of approximately 100 ppbv was found. Note that a detection limit of 0.1 ppbv in N_2 was extrapolated based on noise consideration, absorption coefficient, laser power, and assumed absence of interfering gases. The 100-ppbv detection limit was sufficient to measure the water vapor release from small insects.

6. Performance for Biological Measurements

The dimensions of the buffers of the PA cell (100-mm diameter, 100-mm length) resulted in a total cell volume of 1.5 L. Since we introduced the trace gas flow at the center of the resonator the time response of the detector depended mainly on the volume of the resonator (26 mL). The small diameter gas inlet (0.8 mm) that we used did not influence the cell constant. Acoustic outside noise was effectively suppressed by acoustic notched filters in line with the flow tubes. A notched filter consisted of a small diameter (0.8-mm) and a large diameter (8-mm) tube both of a quarter acoustic wavelength. The noise reduction of such a filter was proportional to the ratio of the cross-sectional areas.[28] The noise reduction by one filter yielded an attenuation factor of 100. During our experiments we used two of these filters, although one filter would have been sufficient.

We tested the properties of PFA Teflon for water memory effects by injecting water vapor into a 5-L/h flow of air and comparing this with injections of methane. The detector had the same time response (15 s) for both trace gases. By switching from a calibrated high concentration trace gas mixture (1.2-ppmv C_2H_4 in N_2) to a pure N_2 flow (1 L/h) we observed 15% of the initial trace gas signal after the first hour. This can be explained by backdiffusion from the buffer volumes into the resonator. After having passed through the resonator the residence time of the trace gas in the buffers was typically 1.5 h. Because of backdiffusion former fillings contribute to the actual

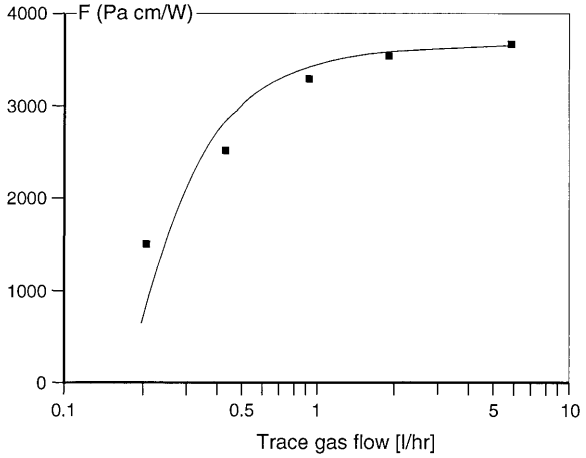

Fig. 5. Comparison between the experimental (filled squares) and theoretical (curve) PA signals generated in the resonator as a function of the trace gas flow (1-ppmv ethylene in nitrogen and resonant CO_2 laser transition at 949.749 cm^{-1}). The buffers are flushed with pure nitrogen. At a low flow rate the undiluted nitrogen diffuses back into the resonator, decreasing the effective absorption length. At a high flow rate the cell constant is equal to the value obtained when the whole cell is filled with trace gas.

signal and cause fairly constant background signal decay on a time scale of hours. One can describe this effect by relating the trace gas flow velocity ($v = 0.02$ cm s^{-1}) to the average distance (d) of backdiffusion into the resonator at stationary conditions, $d = D/2v$ (diffusion constant $D = 0.185$ cm^2 s^{-1} for N_2).

We performed an extracavity experiment employing the above-mentioned CO_2 waveguide laser arrangement to elucidate this problem. We flushed the buffers of the PA cell with N_2 and varied the trace gas flow velocity. Under these conditions backdiffusion of pure N_2 diminishes the PA signals that otherwise would be independent of the flow rate. The influence of the flow rate on the signal amplitude is shown in Fig. 5. The theoretical cell response curve was simulated by the aid of a computer model[22,23] that combined the individual absorption contributions of parts of the resonator tube to a total pressure amplitude at the site of the microphone. This approach yields a good description of this undesired effect. At a flow rate of 0.5 L/h the direct trace gas signal yields only 70% of the PA signal at a flow rate of 6 L/h. Thus, backdiffusion could be reduced significantly by increasing the flow velocity. This is, however, not always desirable since, in the case of a biological source, the production rate becomes diluted at high flow velocities and reduces the concentration. A minimal flow rate of 1 L/h was used for the measurements on biological samples.

To allow for measurements from low production sources with a low carrier gas flow, the gas in the buffers could be purged by additional gas flows of 3 L/h through each buffer. Note that signal reduction by backdiffusion would still take place; the problem of memory effects from trace gas dwelling in the buffer volumes, however, could be reduced by a factor of 5. To balance the buffer in and out flow with the trace gas flow we had to monitor the flow rates carefully so that serious problems were not introduced into the system. When we performed the measurements on insects we used trace gas flows of 1 and 5 L/h in the resonator and 3 L/h to purge the buffers.

The sample gas flowed over the insect as it entered and left the cuvette by way of capillaries. The animals were kept at ambient temperature (22 °C) inside the glass cuvette (20-mm diameter, 50-mm length), which was sealed at both ends with butyl rubber stoppers. We constructed a cooling trap to remove water vapor from the carrier gas. Thus a dry air flow into the sampling cuvette was obtained for determination of the water vapor release; we positioned the trap behind the sampling cuvette to monitor the release of CH_4 by the animal. The cooling trap consisted of trapping stages and a reservoir in which the liquid-nitrogen level was kept constant. Close to the bottom, just above the liquid-nitrogen level of the Dewar, we maintained a metal plate at a constant temperature of 125 K. Near the top we observed a freezing stage of 255 K. The trace gas containing water vapor was first guided through a relatively wide PFA tube (11-mm diameter, 60-mm length) connected to a 255-K plate. At this point most of the water vapor was frozen and, since the tube was easily accessible, we were able to defrost it every day to prevent blockage. For further reduction of the water vapor concentration the flow was guided through a 1-m long (1.6-mm diameter) tube connected to a 125-K plate. Inlet and outlet tubes of the cooling trap consisted of PFA with 0.8-mm diameter (2-m total length).

We performed measurements of CH_4 by periodically switching between two laser lines, one at a strong and the other at a weak methane absorbing line. We used the $P(9)_{32}$ ($\alpha = 0.02$ atm^{-1} cm^{-1}) and the $P(10)_{32}$ ($\alpha = 3$ atm^{-1} cm^{-1}) transitions of CO at 1308.01 and 1304.97 cm^{-1} (see also Fig. 3). We accomplished fast response measurements by keeping the laser at the strong absorption line without switching. We also performed fast water vapor measurements at one single laser line $P(11)_{19}$ transition ($\alpha = 0.3$ atm^{-1} cm^{-1}). Because of the nonlinear dependence of the PA signal on the water vapor concentration the calibration needed special care. At the start and the end of each biological measurement we used injections of saturated water vapor to calibrate on top of the signal emitted by the animal (see, e.g., Fig. 4).

The fast time response measurements included the determination of CO_2 release. The gas flow was thus split; one half was guided to a conventional CO_2 infrared gas analyzer (ultrarot absorption 2T, Hartmann & Braun, Frankfurt, Germany) and the other to a PA cell. After installation we synchronized the detectors utilizing the injection of a CO_2/CH_4 or CO_2/H_2O mixture into the sampling cuvette. When we adjusted the flow resistances at the outlet of the detectors we obtained equal time responses (and delays) of the injected amount. One can calibrate the detec-

tors by injection of a specified amount of CH_4, H_2O, or CO_2.

7. Gas Exchange Measurements of Insects

Some 300 million years ago, long before land-dwelling vertebrates evolved, insects appeared on Earth. These have been estimated to consist of more than two million species and are known to constitute an enormous biomass worldwide. Insects and millipedes contribute to the global change of the atmosphere. Evidently, they all release CO_2 and H_2O and consume O_2 as a natural consequence of their metabolism and breathing. In addition, however, millipedes and at least three higher taxa of insects, termites, cockroaches, and scarab beetles, emit CH_4 as one of the end products of their intestinal (bacteria-aided) fermentations. Estimates show that nowadays total arthropod emission could constitute as much as 25% of the mondial methane production. Our initial use of the described detector was to monitor the emission of methane and water vapor from cockroaches and scarab beetles.

In the anaerobic hindgut of CH_4-producing insects, large numbers of bacteria and symbiotic protozoa assist the digestion of biopolymers such as cellulose or hemicellulose. These metabolic activities are fermentations; they take place under anaerobic conditions and yield CO_2 and H_2 as the main products of biopolymer catabolism, to be converted to CH_4 by methanogenic bacteria that also live in the hindgut of their hosts, either free around the partially digested food particles or as intracellular symbionts of intestinal protozoa. In some instances, the insect forms chitinous structures as immobilized supports for intestinal bacteria.

Gas chromatography permits a quantitative cumulative determination of gas emissions; because of a lack of time resolution, no answer could be given to the question of how the intestinal gases are released. Measuring CH_4 simultaneously with CO_2 enabled us to discriminate between a CH_4 release as flatus or as a breathing product.

Insects such as vertebrates consume O_2 and release CO_2 during respiration. However, insects do not possess lungs; they use a tracheal system for gas exchange. This tracheal system consists of a ramifying system of tubes that connect the internal tissues by way of spiracle valves to the atmosphere (see Fig. 6). The spiracle valves are controlled by muscles through which the ventral nervous system can isolate the tracheal system from the atmosphere. Similar to other cockroaches, *Periplaneta americana* possesses ten pairs of spiracle valves. Gas exchange between the tracheal system and the atmosphere can take place by active ventilation and by diffusion (no movement). The widespread opinion that insects at rest depend solely on diffusion for gas exchange is based on a model postulated by Krogg[29] and investigated by Hazelhoff.[30] It had been assumed that cockroaches ventilate only during motoric activity; at rest, it was deemed that they did not ventilate at all but exchanged gases by diffusion. However with the aid of diaferometric techniques a cyclic CO_2 release and O_2 intake were also observed in resting insects.[31] Insects released CO_2 in bursts whereas O_2 was absorbed at an almost constant rate. These animals developed a complex breathing pattern presumably to retain their body water vapor.[32] This idea was verified by the observation of Kestler that some insects at rest actively ventilate to exchange gases.[14]

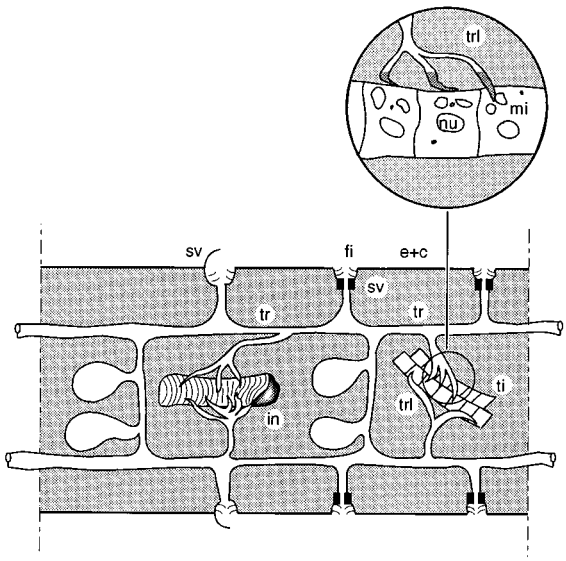

Fig. 6. Schematic view of the tracheal system of an insect. Trachea (tr) connect the oxygen-consuming and CO_2-producing tissues (ti + in) with the ambient atmosphere; (mt) indicates mitochondria. The contact between (tr) and (ti) is accomplished by thin tracheoles (trl). Hemolymph, i.e., insect blood, surrounds tissues and trachea. The trachea are fixed to the epidermis (e) and cuticula (c). The gas exchange is controlled by interior and exterior spiracle valves (sv), which are sometimes protected by a filter (fi).

During the breathing cycles of insects, three periods can be distinguished that are described briefly.[14,32] During the constriction phase (*C*) the spiracle valves are closed; no significant tracheal gas exchange with the atmosphere takes place. The oxygen present in the tracheal system is consumed. The solubility of CO_2 in water is 20-fold higher than that of O_2. CO_2 produced by insect metabolism easily dissolves in the hemolymph that surrounds the tissues. The hemolymph fluid is like the blood for mammals with the exception that there is no major pumping mechanism. Because of oxygen consumption the pressure in the tracheal system drops below the atmospheric value. When the O_2 concentration reaches the lower limit O_2 must be absorbed from the outside.

During the second period (fluttering *F*) the spiracles open for only a short time allowing a convective influx of air in accordance with tracheal gas under pressure. On the average O_2 is taken in and consumed at a constant rate. Only minor amounts of CO_2 are released, since it has to diffuse against the inrushing air. Therefore, the CO_2 concentration in the hemolymph continues to increase.

At a specific moment an increase of the exchange of tracheal gases with the atmosphere can be observed. When the spiracle valves are open, the gas exchange takes place by active ventilation (*V*) because of the movements of the abdomen (the posterior part of the insect). One active pumping volley consists of a rapid expiratory stroke, a maintained compression, and then inhalation. This constriction–fluttering–ventilation (CFV) cycle provides the cockroach with the necessary O_2 and allows the metabolic CO_2 to escape to the atmosphere. Note that in parallel gas exchange takes place by the cuticula (the skin); in particular, this leads to water loss and CO_2 release.

8. Biological Results

Figure 7(a) shows a characteristic methane release pattern of a *Periplaneta americana* cockroach. During this experiment we switched the grating of the laser between two positions; the time resolution was, therefore, only 2 min. The background signal was constant during the course of the measurement, so that the difference signal was due to methane. Nearly five complete cycles are displayed. Within one cycle three periods can be distinguished; a minimum release (*C*) close to the baseline that lasts for approximately 3 min, followed for 20 min by a slowly increasing signal that levels off (*F*), and a burst of methane over a period of 6 min (*V*).

For another *Periplaneta americana* cockroach simultaneous PA measurements of methane on one laser line and of CO_2 with an infrared gas analyzer are shown in Fig. 7(b). The level of CH_4 release is 1 order of magnitude higher than for the cockroach in Fig. 7(a). These differences of 1 order of magnitude were frequently observed for single cockroaches. In Fig. 7(b) the cycles of methane and CO_2 releases took less time (17 min). Both CH_4 and CO_2 exhibit all the characteristics of a CFV breathing pattern.[14] The minimum corresponds to *C*, followed by an increased release rate denoted by *F*. The burst *V* signifies the period during which the cockroach ventilates. Release of CH_4 and CO_2 shows synchronous but slightly different patterns. The onset of *V* is somewhat delayed for CO_2. The ratio of releases during *F* and *V* is much larger for CO_2 than for CH_4. CO_2 emission shows a gradual decrease toward the next constriction period. In contrast, methane stays at a constant level until the start of *C*. Note that no corrections were applied for the background contribution.

Figure 7(c) shows water vapor release by a third *Periplaneta americana*. The water vapor signal shows an offset that is due to continuous release from the animal, probably caused by cuticular losses. Because of the calibration problems with water vapor the scale gives only an indication of water vapor. A possible scale of a factor of 1.5 seems realistic. Released patterns of CO_2 and H_2O that are the result of breathing are almost identical. The changing baseline for the CO_2 released pattern is the result of a drift of the signal in the infrared gas analyzer.

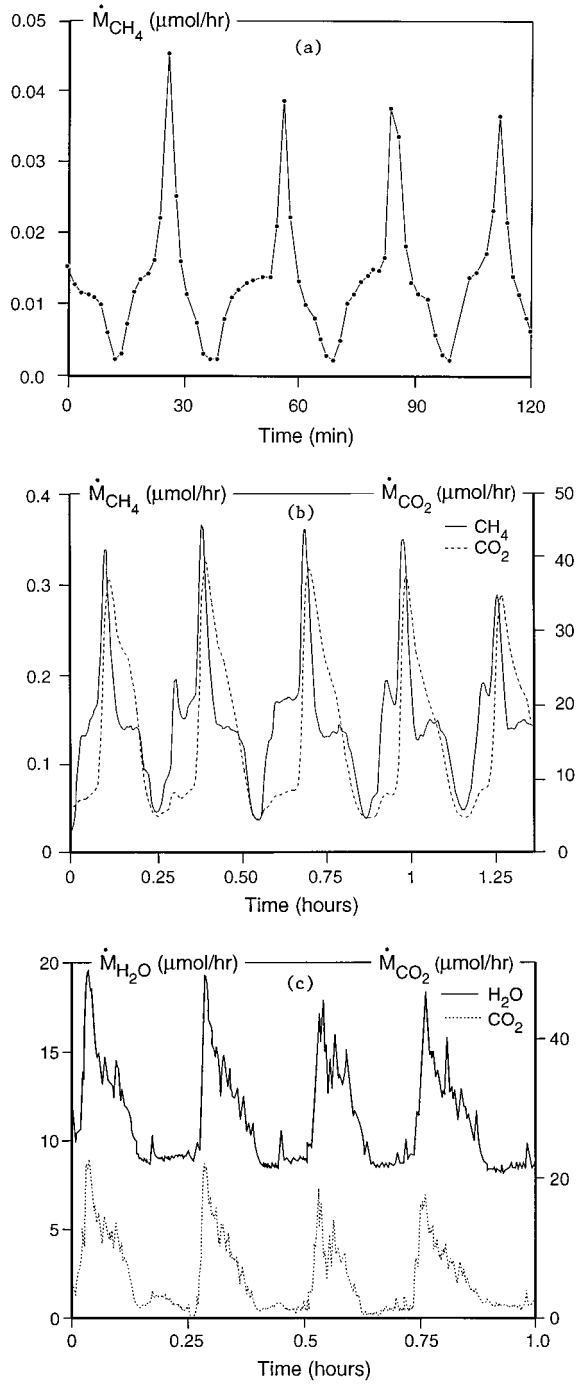

Fig. 7. CH_4, H_2O, and CO_2 release patterns of the *Periplaneta americana* cockroach (40 mm long, fresh weight 1 g). (a) CH_4 release was measured by switching between two adjacent laser lines, one strongly $[P(10)_{32}]$ and one weakly $[P(9)_{32}]$ absorbing line. Time resolution was limited by the switching (2 min) and not by the flow in the PA cell (1 L/h). (b) The total flow rate (5 L/h) over the animal was split into two parts, one entered the infrared gas analyzer (4 L/h) for CO_2 detection; the other (1 L/h) entered the PA cell for CH_4 monitoring. Both gases were measured with an increased time resolution of 15 s since CH_4 was determined at only one laser line $[P(10)_{32}]$. The synchronous observation indicates that methane was released during the breathing of the animal. The phase shift is connected to the higher solubility of CO_2 in the hemolymph. (c) H_2O and CO_2 were measured simultaneously at a total flow over the animal of 10 L/h (split into two equal parts).

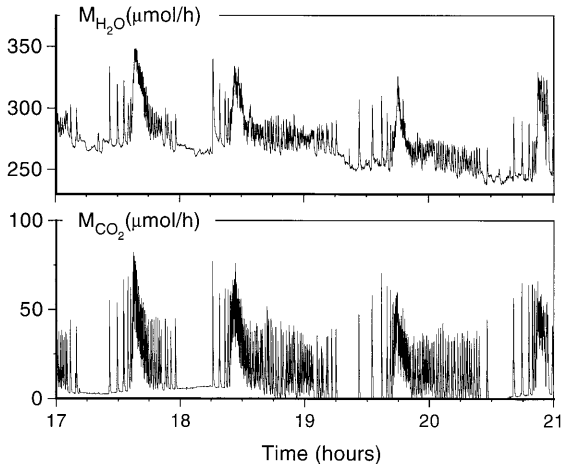

Fig. 8. Almost five breathing cycles from a *Gromphadorhina portentosa* cockroach (50 mm long, fresh weight 6 g). A high water vapor background signal was observed due to diffusive cuticular release. Three characteristic CFV periods of insect breathing can be distinguished: constriction (17.2–17.4 h), fluttering (17.4–17.6 h), and ventilation (17.6–18.0 h). Note the perfectly synchronized release with CO_2. The H_2O and CO_2 releases were measured with a time resolution of 15 s (5-L/h PA cell and 5-L/h infrared analyzer).

Figure 8 shows the release of CO_2 and water vapor by a giant (6-g) *Gromphadorhina portentosa* cockroach. The same characteristic CFV cycle can be observed as for *Periplaneta americana* but during (V) single pumping volleys are resolved as peaks caused by active ventilation. The full width at half-maximum of these peaks corresponds to the time response of the detector (15 s). The individual cycles last for approximately 1 h; all the features are synchronous for the release of CO_2 and H_2O.

A different release pattern was found for the *Pachnoda bhutana* scarab beetle for which methane and CO_2 releases were observed to occur synchronously [Fig. 9(a)]. Every 1.5 h a large amount of CO_2 and CH_4 was released in a single burst that lasted for approximately 6 min [see Fig. 9(b)]. A CH_4 burst lasted for a shorter period of time than did a CO_2 burst. Figure 9(c) displays the water vapor release in combination with CO_2 from another scarab beetle. After the start of the measurement the water vapor background release showed a slowly decaying release rate. Except for the larger background signal the water vapor release revealed a pattern similar to that

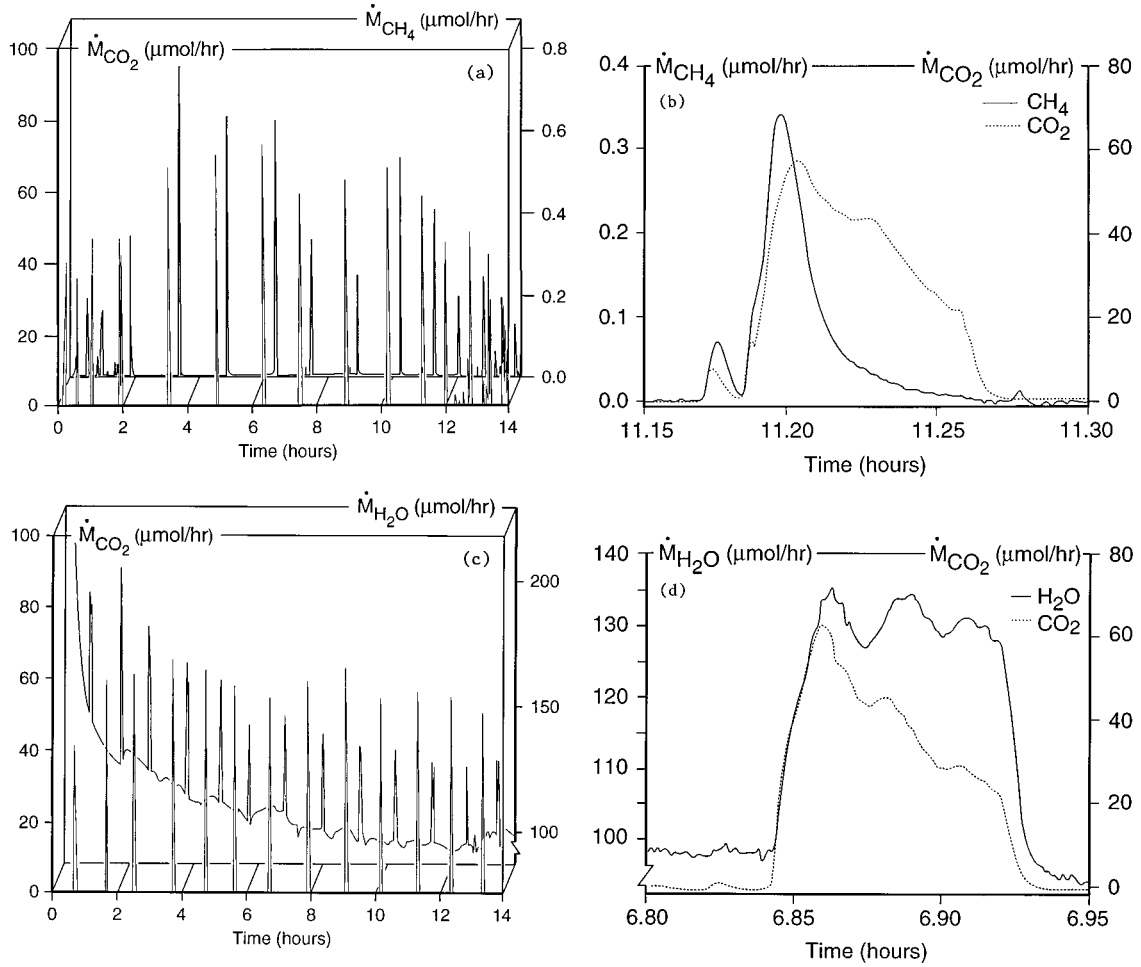

Fig. 9. CH_4, H_2O, and CO_2 release patterns during the breathing of a scarab beetle. Flow conditions as in Fig. 8. (a) CH_4 and CO_2 release patterns for a one night period; note that in the morning when people arrived (12 h after the experiment was started) the beetle became restless. (b) Extended view of one breathing pulse from (a). (c) Concomitant H_2O and CO_2 release patterns during another night period. (d) Extended view of one breathing pulse from (c).

of CH_4 and CO_2. Expansion of the horizontal scale shows, however, that in contrast to CO_2 and ethane the water vapor release was almost constant during a burst.

All the release patterns presented in Figs. 7–9 show that CH_4, CO_2, and H_2O were emitted synchronously. Therefore, the cyclic release of CH_4, in particular, can be attributed to tracheal gas exchange, which proves that methane is not emitted by flatulence. Cyclic water vapor release was observed on top of a fairly constant background signal that has been attributed to cuticular water losses.

Gas exchange that is due to ventilation is accompanied by exhalation of gas. The time response of the system (15 s) allowed us to identify only the gas release of individual pumping volleys in the release pattern of *Periplaneta americana*. The peaks of gas release from *Gromphadorhina* are better resolved and demonstrate clearly that this animal ventilates for its gas exchange.

For *Pachnoda bhutana* the slow decay in water vapor background release is caused by the change of humid ambient to arid conditions in the cuvette at the start of the measurement. The exterior parts of the animal still retain a relatively high amount of water that is slowly released under the arid conditions in the cuvette. The burst period of the gas release does not seem to allow for ventilation and gas exchange seems to be diffusive. The different release patterns for the three gases during the burst cannot be explained solely by their different diffusion coefficients. The CH_4 molecules and water vapor possess equal mass and show similar release patterns whereas CO_2 (since it is heavier) yields a slower decay. Other mechanisms must be involved to explain the different release patterns.

The almost constant water vapor release during the burst suggests that the beetle keeps its valves open constantly and that inside the tracheal system there is a fairly constant partial pressure of H_2O close to the saturation pressure. The slow decrease of CO_2 release during the burst is caused by continuous emission of the CO_2 dissolved in the hemolymph. In contrast, the release of CH_4, practically undissolved in the hemolymph, occurs 1 order of magnitude faster. For methane, refilling the tracheal system occurs less efficiently than for CO_2 because of the order of magnitude difference in solubility.

9. Conclusions

An intracavity photoacoustic cell inside the resonator of a liquid-nitrogen-cooled CO laser was employed to measure trace gas release (H_2O and CH_4). By differential trapping of possibly interfering water vapor (for CH_4 at 125 K, after which the major part of H_2O was removed at 255 K) we detected methane essentially as a one-component-in-air detection. For fast measurements we used laser radiation from a single laser transition whereas for more precise determination we used the difference between two laser wavelengths for which the sampling time increased from 15 s to 2 min. The PA cell was especially designed to minimize wall effects and window signals. Water showed a nonlinear dependence on concentration, a surprising result traced back to kinetic cooling. Oxygen molecules with their high number density and their slow relaxation act as a vibrational energy buffer and transfer the energy into translational energy by collisions preferentially with water molecules.

The CH_4 signal also appeared to be strongly influenced by the presence of traces of H_2O. Again, oxygen played a detrimental role as an energy buffer. Detection limits of 10 ppbv in dry air and 1 ppbv in nitrogen were obtained. For water vapor the detection was limited by the amount of background H_2O vapor present in the cell allowing a detection limit of approximately 100 ppbv. Measurements of living insects revealed that the time response (15 s) of the instrument was sufficient to detect characteristic breathing patterns of cockroaches and scarab beetles. For the first time, to our knowledge, methane was found to be released through breathing.

We thank C. Sikkens, F van Rijn, and R. Kasman for excellent technical support and the Dutch Technology Foundation for generous financial support.

References

1. P. L. Meyer and M. W. Sigrist, "Atmospheric pollution monitoring using CO_2 laser photoacoustic spectroscopy and other techniques," Rev. Sci. Instrum. **61,** 1779–1807 (1990).
2. L. B. Kreuzer, "Ultralow gas concentration infrared absorption spectroscopy," J. Appl. Phys. **42,** 2934–2943 (1971).
3. M. Fiedler, C. Golz, and U. Platt, "Nonresonant photoacoustic monitoring of atmospheric methane," in *Optical Methods in Atmospheric Chemistry*, H. I. Schiff and U. Platt, eds., Proc. SPIE **1715,** 212–221 (1992).
4. T. H. Vansteenkiste, F. R. Faxvog, and D. M. Roessler, "Photoacoustic measurement of carbon monoxide using a semiconductor diode laser," Appl. Spectrosc. **35,** 194–196 (1981).
5. S. B. Tilden and M. B. Denton, "A comparison of data reduction techniques for line-excited optoacoustic analysis of mixtures," Appl. Spectrosc. **39,** 1017–1022 (1985).
6. T. X. Lin, W. Rohrbeck, and W. Urban, "Long wavelength operation of a CW CO-laser up to 8.18 μm," Appl. Phys. B **26,** 73–76 (1981).
7. T. George, S. Saupe, M. H. Wappelhorst, and W. Urban, "The CO fundamental-band laser as secondary frequency standard at 5 μm," Appl. Phys. B **59,** 159–166 (1994).
8. B. Wu, T. George, M. Schneider, W. Urban, and B. Nelles, "Development of a new CW single line CO laser on the $v' = 1 \rightarrow v'' = 0$ band," Appl. Phys. B **52,** 163–167 (1991).
9. W. Urban, "Infrared lasers for spectroscopy," in *Frontiers of Laser Spectroscopy of Gases*, A. C. P. Alves, J. M. Brown, and M. Hollas, eds. (Kluwer, Deventer, The Netherlands, 1988), pp. 9–42.
10. S. Bernegger and M. W. Sigrist, "CO-laser photoacoustic spectroscopy of gases and vapors for trace gas analysis," Infrared Phys. **30,** 375–429 (1990).
11. F. G. C. Bijnen, T. Brugman, F. J. M. Harren, and J. Reuss, "A liquid nitrogen cooled CO laser in a photoacoustic setup monitors low gas concentrations," in *Photoacoustic and Photothermal Phenomena III*, D. D. Bicanic, ed. (Springer-Verlag, Heidelberg, 1992), pp. 34–37.
12. J. E. Rogers and W. B. Whitman, *Microbial Production and Consumption of Greenhouse Gases* (American Society for Microbiology, Washington, D.C., 1991), pp. 7–38.

13. J. H. P. Hackstein and C. K. Stumm, "Methane production in terrestrial arthropods," Proc. Natl. Acad. Sci. U.S.A. **91,** 5441–5445 (1994).
14. P. Kestler, "Respiration and respiratory water loss," in *Environmental Physiology and Biochemistry in Insects*, K. H. Hoffmann, ed. (Springer-Verlag, Berlin, 1985), pp. 137–183.
15. M. C. Quinlan and N. F. Hadley, "New system for concurrent measurement of respiration and water loss in arthropods," J. Exp. Zool. **222,** 255–263 (1982).
16. J. R. B. Lighton, D. Garrigan, F. D. Duncan, and R. A. Johnson, "Respiratory water loss during discontinuous ventilation in queens of the harvester ant *Pogonomyrmex rugosus*," J. Exp. Biol. **179,** 233–244 (1993).
17. E. B. Edney, *Water Balance in Land Arthropods* (Springer-Verlag, New York, 1977).
18. C. E. Treanor, J. W. Rich, and R. G. Rehm, "Vibrational relaxation of anharmonic oscillators with exchange-dominated collisions," J. Chem. Phys. **48,** 1798–1807 (1968).
19. J. W. Rich, "Kinetic modeling of the high-power carbon monoxide laser," J. Appl. Phys. **42,** 2719–2730 (1972).
20. G. A. Murray and A. L. S. Smith, "Plasma kinetic effects of the addition of oxygen to CO laser discharges," J. Phys. D **14,** 1745–1756 (1981).
21. F. J. M. Harren, J. Reuss, E. J. Woltering, and D. D. Bicanic, "Photoacoustic measurements of agriculturally interesting gases; detection of C_2H_4 below the ppb level," Appl. Spectrosc. **44,** 1360–1368 (1990).
22. F. G. C. Bijnen, "Refined CO laser photoacoustic trace gas detection; observation of anaerobic processes in insects, soil and fruit," Ph.D. dissertation (University of Nijmegen, Nijmegen, The Netherlands, 1995).
23. F. G. C. Bijnen, F. J. M. Harren, and J. Reuss, "Geometrical optimization of a longitudinal resonant photoacoustic cell; sensitive and fast trace gas detection with applications on gas emission from tomatoes," Rev. Sci. Instrum. **67** (July 1996).
24. F. G. Gebhardt and D. C. Smith, "Kinetic cooling of a gas by absorption of CO_2 laser radiation," Appl. Phys. Lett. **20,** 129–132 (1972).
25. R. A. Rooth, A. J. L. Verhage, and L. W. Wouters, "Photoacoustic measurement of ammonia in the atmosphere: influence of water vapor and carbon dioxide," Appl. Opt. **29,** 3643–3653 (1990).
26. E. Avramides and T. F. Hunter, "Vibrational–translational/rotational and vibrational–vibrational processes in methane: optoacoustic measurements," Chem. Phys. **57,** 441–451 (1981).
27. J. D. Lambert, *Vibrational and Rotational Relaxation in Gases* (Clarendon, Oxford, 1977).
28. C. M. Harris, ed., in *Handbook of Noise Control* (McGraw-Hill, New York, 1957), Chap. 21.
29. A. Krogh, "Studien über Tracheenrespiration. II. Uber Gasdiffusion in den Tracheen," Pfluegers Arch. Gesamte Physiol. Manschen Tiere **179,** 95–112 (1920).
30. E. H. Hazelhoff, "Regeling der ademhaling bij insecten en spinnen," Ph.D. dissertation (State University Utrecht, Utrecht, The Netherlands, 1926).
31. A. Punt, W. J. Parser, and J. Kuchlein, "Oxygen uptake in insects with cyclic CO_2 release," Biol. Bull. Woods Hole, Mass. **112,** 108–119 (1957).
32. R. I. Levy and H. A. Schneiderman, "Discontinuous respiration in insects IV. Changes in intratracheal pressure during the respiratory cycle of silkworm pupae," J. Insect Physiol. **12,** 465–492 (1966).